2007-04-24

Coupling Down Converted Light Into Single Mode Fibers

David A. Niemi
Brigham Young University - Provo

COUPLING DOWN CONVERTED LIGHT INTO SINGLE MODE FIBERS

by

David Niemi

A thesis submitted to the faculty of

Brigham Young University

in partial fulfillment of the requirements for the degree of

Master of Science

Department of Physics and Astronomy

Brigham Young University

August 2007

BRIGHAM YOUNG UNIVERSITY

GRADUATE COMMITTEE APPROVAL

of a thesis submitted by

David Niemi

This thesis has been read by each member of the following graduate committee and by majority vote has been found to be satisfactory.

Date	Michael Ware, Chair
Date	Justin Peatross
Date	Jean-Francois Van Huele

BRIGHAM YOUNG UNIVERSITY

As chair of the candidate's graduate committee, I have read the dissertation of David Niemi in its final form and have found that (1) its format, citations, and bibliographical style are consistent and acceptable and fulfill university and department style requirements; (2) its illustrative materials including figures, tables, and charts are in place; and (3) the final manuscript is satisfactory to the graduate committee and is ready for submission to the university library.

Date

Michael Ware
Chair, Graduate Committee

Accepted for the Department

Scott Sommerfeldt, Chair
Department of Physics and Astronomy

Accepted for the College

Thomas W. Sederberg, Associate Dean
College of Mathematics and Physical Sciences

ABSTRACT

COUPLING DOWN CONVERTED LIGHT INTO SINGLE MODE FIBERS

David Niemi

Department of Physics and Astronomy

Master of Science

We investigate the influence of the pump and collection mode parameters on the collection efficiency of Type I down converted photons into single mode fibers. For best single and coincidence counting rates, we find that the mode sizes should be close to the same size and that the mode waists should be located near the down-conversion crystal. Larger collection waists give higher collection efficiencies, but lower singles counts.

ACKNOWLEDGMENTS

Thanks to Michael Ware, Justin Peatross, and Jean-Francois Van Huele for their support and friendship. I wish to express appreciation to my parents, Tim and Catharine Niemi, as well as Charles Niemi, Jeff Niemi, and Miriam Weinrich for their love, support, and encouragement.

Contents

Chapter 1

Introduction

The field of quantum optics was born when Max Plank, reluctantly, assumed that light energy is quantized [1] in an effort to explain blackbody radiation. Although Planck felt uncomfortable with this description of light, a century of experimental and theoretical work has shown it to be accurate. From Einstein's description of the photoelectric effect to recent applications such as quantum computing [2], quantum cryptography [3, 4], and quantum teleportation [5] the predictions of quantum optics have been shown to be valid, and extremely useful.

In this thesis we investigate the coupling of down-converted light quanta into single mode fibers. This study relates to a number of potential quantum optics applications, but is particularly useful in creating single photon sources for use in quantum cryptography and quantum computing. Section 1.1 briefly reviews these applications and in section 1.2 we review the current available single photon sources. Then in section 1.3 we discuss the need to study the coupling of down converted light into single mode fibers. In section 1.4 we present the basic theory of parametric down-conversion, and in section 1.5 we consider some modifications to the basic theory that will affect our experiment. Finally, in section 1.6 we will review some of the previous

work done in coupling down-conversion into fiber optics.

1.1 Single Photon Applications

Quantum Cryptography

Cryptography is the study of sending secret messages. The most common use of cryptography in today's society is to secure, from eavesdroppers, transactions between distant parties (usually via the internet). Current public key internet encryption schemes are based on the assumption that it is computationally difficult to split extremely large numbers into their prime factors. If a computer were to be constructed that could factor these extremely large numbers, all current (and recorded past) internet transactions could be read by third parties. Quantum cryptography is arguably the most useful applications of quantum optics to date because it removes this computational loophole from cryptography, making transactions physically, rather than computationally, secure.

Quantum cryptography protocols allow the sharing of information between distant parties in such a way that eavesdropping by a third party is always detectable before any secret information is transmitted. In quantum cryptography information is encoded in the polarized states of a series of single photons. A measurement destroys the photon, but the polarization state of the photon cannot be completely characterized with one measurement. Thus, the eavesdropper is not likely to retransmit a new photon in the same state as the original. By examining the number of errors in the transmission the sender and receiver can determine if someone is eavesdropping. The initial transmission contains only a string of random numbers that will be used as a "key" to encrypt the actual message. If eavesdropping is detected transmission can stop before any sensitive information is transmitted. Thus, this form of communi-

cation makes it, in theory, impossible for an eavesdropper to listen in without being detected.

One protocol for quantum cryptography was invented by Charles Bennett and Gilles Brassard in 1984 [6], referred to as the BB84 protocol. To implement this encryption protocol the sender (Alice) and receiver (Bob) each create a random sequence of numbers. Alice transmits her sequence of random numbers to Bob by sending a photon at regular intervals and randomly choosing one of two polarization bases, $B = \{0°, 90°\}$ or $D = \{45°, 135°\}$. Bob uses his random sequence to choose which basis to measure in. Because the sending basis and detection basis are both chosen at random, half of the time (on average) Bob will measure in the wrong basis. As Alice transmits, Bob makes his measurements and records his results. After transmitting a number of photons, Alice and Bon compare the sequence of bases that they have used, and throw out the measurement made when the photons were not sent and received in the same basis. The results of the measurements made in the same basis form the key (like a password) used to encrypt the information transmitted through a classical channel.

In implementing the BB84 protocol, or any other quantum encryption scheme, it is important to use a single photon source. If two or more photons are transmitted at the same time then one could potentially be intercepted by an eavesdropper. Since the receiver would have no way of detecting the eavesdropper's presence, this compromises security. It is also important to transmit a photon at regular intervals so the receiver knows when to look for the incoming photon. Quantum cryptography systems using attenuated lasers as their single-photon source are now commercially available, but would be benefited by an improved single photon source.

Optical Quantum Computing

Another application with great potential in quantum optics is the construction of a quantum computer. The main driver behind quantum computing is Shor's algorithm, which allows a quantum computer to quickly factor very large numbers into their primes. As previously discussed, current public key internet encryption schemes are based on the assumption that this operation is computationally too difficult to be done by digital computers in a reasonable time. Thus, if a quantum computer were available, one could decrypt most of the messages sent via the internet. The threat of this capability is what drives the field of quantum cryptography. In addition to the factoring ability, other algorithms have been devised for quantum computers, such as performing fast searches on randomly organized data [7].

There are many technical problems that must be overcome in order to build a quantum computer, and to date no scalable quantum computers have been realized. Quantum computing can be done in a number of mediums, and we will not discuss all aspects of this field here. What is relevant to the current discussion is that in order to build a quantum computer, it is essential to have well-defined "qbits". A qbit is a quantum system that has two possible states, analogous to a 0 and 1 in regular digital computing. Unlike classical bits, qbits can be in a superposition of states at the same time. For example, the spin of an electron can be spin up state ($|1\rangle$), spin down state ($|0\rangle$) or in a super position of states.

In order to do quantum computing with photons it is necessary to have a well-defined qbit. In optical quantum computing, this is a single photon where the two possible states are orthogonal polarization states. If there is more than one photon at the same time, there are more than two possible states for the quantum system and it is not a true qbit. An important part of optical quantum computing research is constructing reliable single-photon sources to produce the needed qbits.

1.2 Single Photon Sources

As illustrated in the previous section, in many quantum optics applications it is necessary to produce single photons in a reliable and repeatable manner. This is technically challenging for a number of reasons. The three main single-photon sources used to date are quantum dots, attenuated laser pulses, and parametric down-conversion sources. Each of these sources has advantages and disadvantages.

A quantum dot is a nanoparticle which can have carefully engineered energy states. These quantum dots can act as a push button single photon source [8]. An electron is excited to an energy level, and then decays back down to a ground state of the well emitting a single photon. The advantage of this type of source is that when you get a photon, it will be a single photon. However, the direction of the photon is difficult to control, so the emitted photon is difficult to collect. In addition, the excitation process is usually not completely reliable, so sometimes the quantum dot will not emit any photons to be collected.

Single photons can also be produced by simply attenuating laser pulses to the single photon level. This is certainly the simplest single-photon source, but it has its drawbacks. The number of photons in a given pulse obeys Poisson statistics given by

$$p(n) = \frac{\bar{n}^n e^{-\bar{n}}}{n!}. \tag{1.1}$$

p(n) is the probability of having n photons in a pulse, and $\bar{n}$ is the average number of photons per pulse (experimentally controlled by varying the amount of attenuation). If $\bar{n}$ is chosen to be, say, 1 photon per pulse, then 36.8% of the pulses will have 0 photons (i.e. be empty), 36.8% will have 1 photon, and 26.4% will have more than one (see Fig. 1.1). If $\bar{n} > 1$ then a smaller fraction of the pulses will be empty, but the fraction of pulses that will have more than one photon will increase (i.e., more than 26.4% will be multi-photon). On the other hand if $\bar{n} < 1$ then most of the pulse

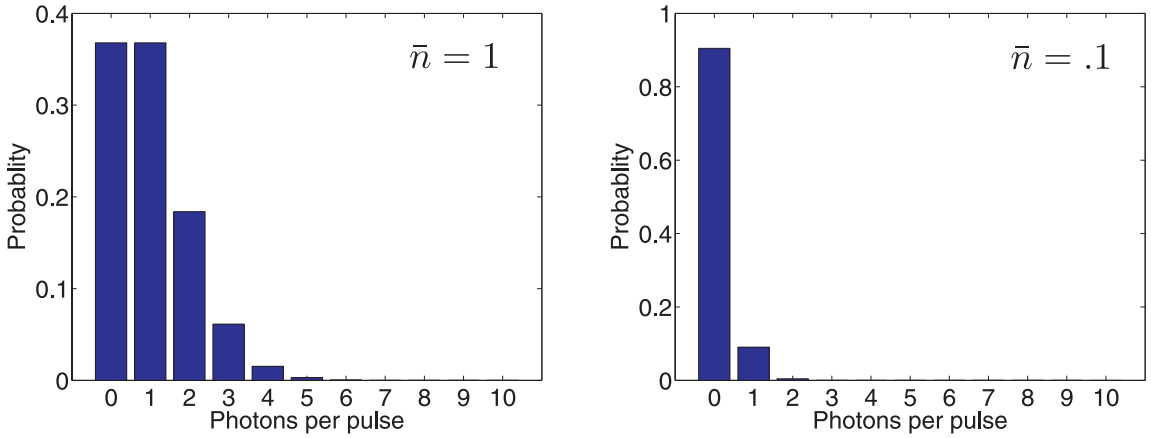

Figure 1.1 Plot of Eq. 1.1 with $\bar{n} = 1$ photons per pulse on the left and $\bar{n} = 0.1$ photons per pulse on the right.

will be empty, but the ratio of single-photon to multi-photon pulses will be better. If we use $\bar{n} = 0.1$ then about 90% of the pulses will be empty, and only about 10% of the pulse have photons (see Fig. 1.1). However, when we do get a pulse with photons in it, we can be much more confident that it is a single photon than was the case for $\bar{n} = 1$.

Another single photon source is based on parametric down-conversion (PDC). In the PDC process, high energy photons essentially "break apart" in an optically nonlinear crystal to produce two lower-energy photons. Since, the photons are always produced in pairs, the detection of one of the down-converted photons heralds with certainty the presence of the other down-converted photon. The process occurs at random, so one never knows when the photon pair will come. However, if the down-conversion source is pumped with a pulsed laser, this allows the experimenter to know when and where to look for a single photon. For example if a picosecond laser pulse is used to create the photons then the experimenter can detect one photon and know where the other photon is because of the conversion of momentum. Among the more famous experiments conducted using PDC is a physical realization [9] of a thought

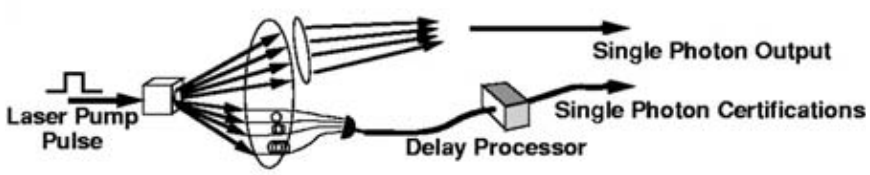

Figure 1.2 A single photon source where half of the down converted light is collected into delay fibers and sent to a detector. While the other half of the light is collected by a lens into one optical fiber. The detector will tell when there is a photon in the optical fiber. Figure taken from [11]

experiment proposed in 1935 by Einstein, Podolsky, and Rosen [10]that demonstrates the nonlocal nature of quantum mechanics.

An enhanced single photon source can be created by collecting some down converted light, created using a pulsed laser, on one side of a down conversion ring into a series optical fibers that delay the photons with respect to each other [11] (see Fig. 1.2). These fibers can be connected to a photon detector that controls an optical switch. When the detector fires we may know that the twin photon is on the other side of the ring. A lens can be used to collect the twin into a single optical fiber. The photon detector triggers an optical switch that allows the twin photons through to an output. This will give more chances to get a single photon. Thus, closely approximating an on demand single photon source.

1.3 The Need to Understand Coupling PDC into Optical Fibers

In quantum computation and cryptography the single photons produced in PDC must be coupled from the original geometry of down-conversion into other optical systems. Learning to efficiently couple this down converted light into single mode fibers would be useful, so that equipment does not have to be specially positioned to collect light

from the down conversion rings. Pump focusing, crystal length, and the collection modes are some of the factors that influence the collection of the down converted light. In our study we consider the effects of pump focusing, and the collection modes.

1.4 Parametric Down Conversion

In the case of a plane wave pump and an infinitely long crystal, conservation of energy and momentum yield a relatively simple description of parametric down-conversion. The momentum of a photon obey $\mathbf{p} = \hbar\mathbf{k}$, so momentum conservation requires

$$\mathbf{k}_\mathrm{p} = \mathbf{k}_\mathrm{s} + \mathbf{k}_\mathrm{i} \tag{1.2}$$

where the subscripts p, s, and i refer to the pump, signal, and idler, respectively. Furthermore, the conservation of energy gives

$$\omega_\mathrm{p} = \omega_\mathrm{s} + \omega_\mathrm{i} \tag{1.3}$$

where ω is the angular frequency of a photon, and is related to the energy of a photon by $E = \hbar\omega$. The index of refraction varies both with frequency and direction in non-isotropic crystals, so there are many combinations of signal and idler photons that satisfy these phase-matching constraints.

Using Eqs. 1.2 and 1.3, we can write a simple *phase-matching function* to describe what combinations of wave-vectors and frequencies result in down-conversion:

$$\Phi_\mathrm{simple} = \delta^3\left(\Delta\mathbf{k}\right)\delta\left(\Delta\omega\right) \tag{1.4}$$

where

$$\Delta\mathbf{k} = \mathbf{k}_\mathrm{p} - \mathbf{k}_\mathrm{s} - \mathbf{k}_\mathrm{i} \qquad \text{and} \qquad \Delta\omega = \omega_\mathrm{p} - \omega_\mathrm{s} - \omega_\mathrm{i} \tag{1.5}$$

The value of the phase-matching function is proportional to the probability that down-conversion will occur for a given set of parameters. Equation 1.4 represents a

very simple relation, but in the next section we will see a more complicated phase-matching function.

In a uniaxial crystal, phase-matching generally occurs (i.e., Eqs. 1.2 and 1.3 are satisfied) when the pump polarization is chosen such that it experiences the ordinary index of refraction. In Type I PDC, the two new photons both have extraordinary polarization. In Type II PDC, one of the photons is polarized along the ordinary axis and the other is polarized along the extraordinary axis. In summary, PDC occurs when we can find wave vectors in the crystal that satisfy

$$\mathbf{k}_{\mathrm{p}}(o) = \mathbf{k}_{\mathrm{s}}(e) + \mathbf{k}_{\mathrm{i}}(e), \tag{1.6}$$

$$\mathbf{k}_{\mathrm{p}}(o) = \mathbf{k}_{\mathrm{s}}(o) + \mathbf{k}_{\mathrm{i}}(e), \text{ or} \tag{1.7}$$

$$\mathbf{k}_{\mathrm{p}}(o) = \mathbf{k}_{\mathrm{s}}(e) + \mathbf{k}_{\mathrm{i}}(o), \tag{1.8}$$

where o means ordinary polarization, and e means extraordinary polarization. Equation 1.6 is for Type I down conversion, while Eqs. 1.7-1.8 are for Type II.

By knowing the indices of refraction of a given crystal, one can predict the direction that the light will come out of the crystal [12]. As a very loose analogy, one can compare the down-conversion process to a ball traveling through space, which breaks up into two pieces (see Fig. 1.3). Conservation of mass in the ball system is analogous to conservation of energy in down-conversion, and conservation of momentum will dictate the direction the pieces can take.

In this thesis we study the case of Type I down-conversion. The angle of the emitted photons (measured with respect to the pump direction) is associated with the k-vector (wavelength). Since the process is asymuthally symmetric rings of color appear. Figure 1.4 shows a color photograph of Type I down-conversion from a KDP crystal pumped with 351 nm light. On the left side is a plot of the numerically predicted angles for the signal and idler photons. The top x axis shows the wavelength

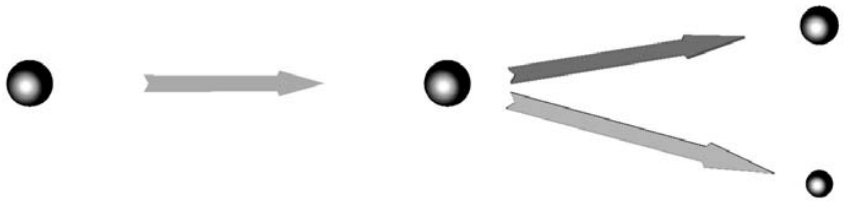

Figure 1.3 A ball travels through space and breaks into two pieces. Conservation of momentum dictates the direction the two pieces must travel. Created by Roy Hammel.

of the signal photons (angles predicted by top curve), while the bottom x axis corresponds to the wavelength of the correlated idler (bottom curve). The two wavelengths are related by writing Eq. 1.3 in terms of the vacuum wavelength of the frequencies:

$$\frac{1}{\lambda_{\mathrm{p}}} = \frac{1}{\lambda_{\mathrm{s}}} - \frac{1}{\lambda_{\mathrm{i}}}. \tag{1.9}$$

For instance, if the signal photon is green (532 nm) then the idler twin will be in the infrared (1032 nm). In Fig. 1.4 the correlated wavelengths can be found by drawing a vertical line connecting the two x-axes. Notice in Fig. 1.4 that the degenerate (same wavelength) photons are at 702 nm, and that the two angles are the same in this case.

1.5 Imperfect Phase Matching

In a lab setup of parametric down-conversion, we of course use finite-length crystals pumped with a laser that has a spatial profile. In this case, the simplified phase matching conditions embodied in Eq. (1.4) no longer strictly hold. Since the photons interact only in the crystal, the finite length puts an uncertainty limit on how well the photons' momenta are defined. When pumping with a pulsed laser, there is also an uncertainty in the pump frequency, and hence the photon energies. For the current analysis, we will assume that the uncertainty in the pump frequency (due to a pulsed pump) is negligible. Furthermore, we assume that the pump beam is Gaussian and

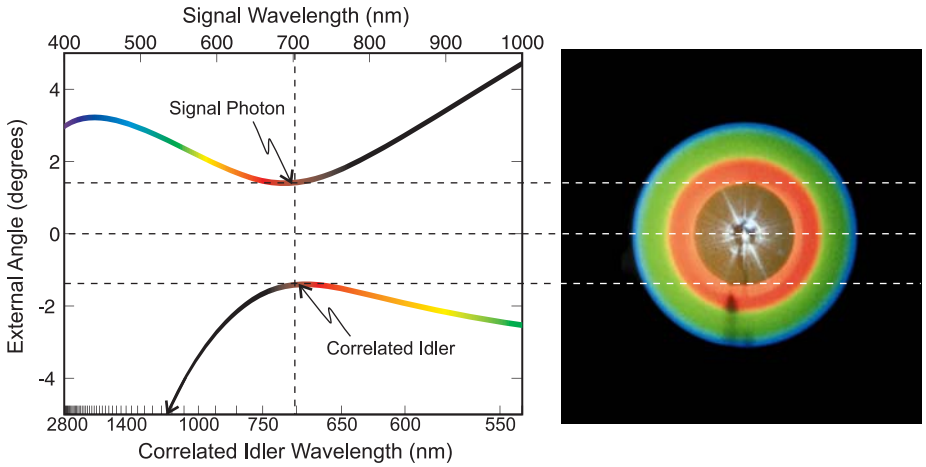

Figure 1.4 The left part of this figure shows where the down converted photons will be located relative to each other. The two x axes shows the wavelength for a given photon, and the wavelength of the twin straight across on the other axis. The right part of this figure is a picture of down conversion rings courtesy of Alan Migdall, NIST.

has a Rayleigh range that is long compared to the length of the crystal, so that we may consider the cross section of the pump as constant throughout the crystal. Under these assumptions, the phase-matching function in Eq. (1.4) is replaced by [12]

$$\Phi = \exp\left(-\frac{w_{\mathrm{p}}^2}{2}(\Delta k_x^2 + \Delta k_y^2)\right) \mathrm{sinc}^2\left(\frac{L\Delta k_z}{2}\right) \delta(\Delta\omega). \tag{1.10}$$

$\Delta k_{x,y,z}$ measures the amount by which Eq. 1.2 is violated, where the pump propagates along the z-axis, x and y are the transverse coordinates. As the pump beam radius w_p and length of the crystal L become infinite then the phase-matching function reduces to the simple case in Eq. 1.4. This equation allows us to pick the location of one of the photons and then direction of the other until we find the likely direction of its twin. The directions with the greatest probability of finding the twin photon corresponds to near perfect phase matching ($\Delta k_{x,y,z} \approx 0$). This function can be used to create plots that predict how the light will come out of our crystal (see Fig. 1.5). By carefully looking at Fig. 1.5 one can see the influence the sinc function has on the plot by observing that there are bright and dark bands away from the main band.

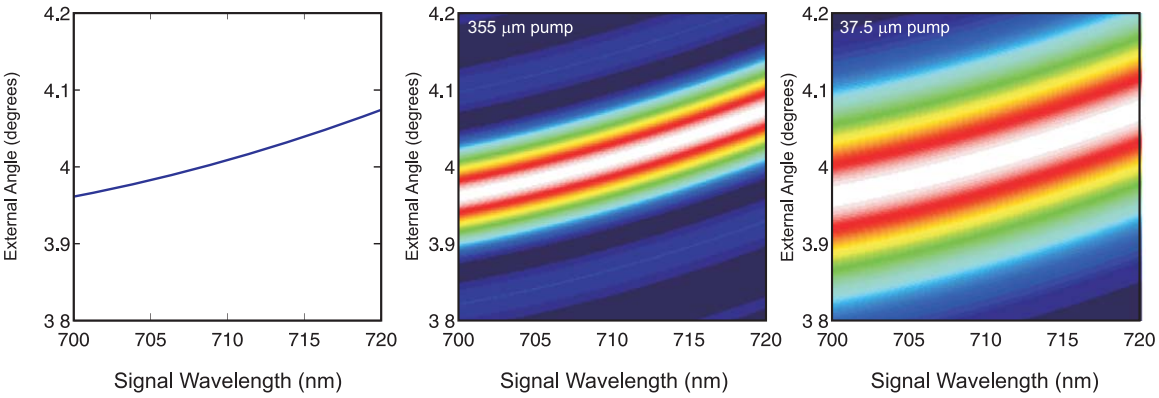

Figure 1.5 Due to imperfect phase matching the curve shown on the left will have some thickness. The amount of spreading is dependent on the waist of the pump beam. The plot in the middle is for a 350 μm waist produced by a 1 m lens. The plot on the right is for a 37.5 μm waist, which corresponds to a 20 cm lens in our pump beam.

The detectors will see certain portions of the down conversion rings because the collection lenses have a finite size, and the filters select a specific bandwidth. To see how this effects the what the detectors see let's consider three types [13] of angular spreading of the down conversion ring. One type of spreading that occurs is that a given wavelength, under perfect phase matching, corresponds to a specific angle (see Fig. 1.6). Each wavelength travels in a specific direction, so our bandpass filter partially controls the range of angles we can detect. Another type of spreading is caused by the mismatching of momentum, which causes more than one angle to correspond to a given wavelength. Finally, the last type of spreading is caused by the beam being finite in size. This means that the pump beam is not a plane wave, but composed of many plane waves. As a result when the beam is sharply focused the down conversion rings will be wider than if the beam is collimated Fig. 1.6 accounts for all types of spreading, and in particular demonstrates the effect of focusing the pump beam.

In Fig. 1.6 we assumed perfect phase matching by using Eqs.1.3-1.6. Looking at

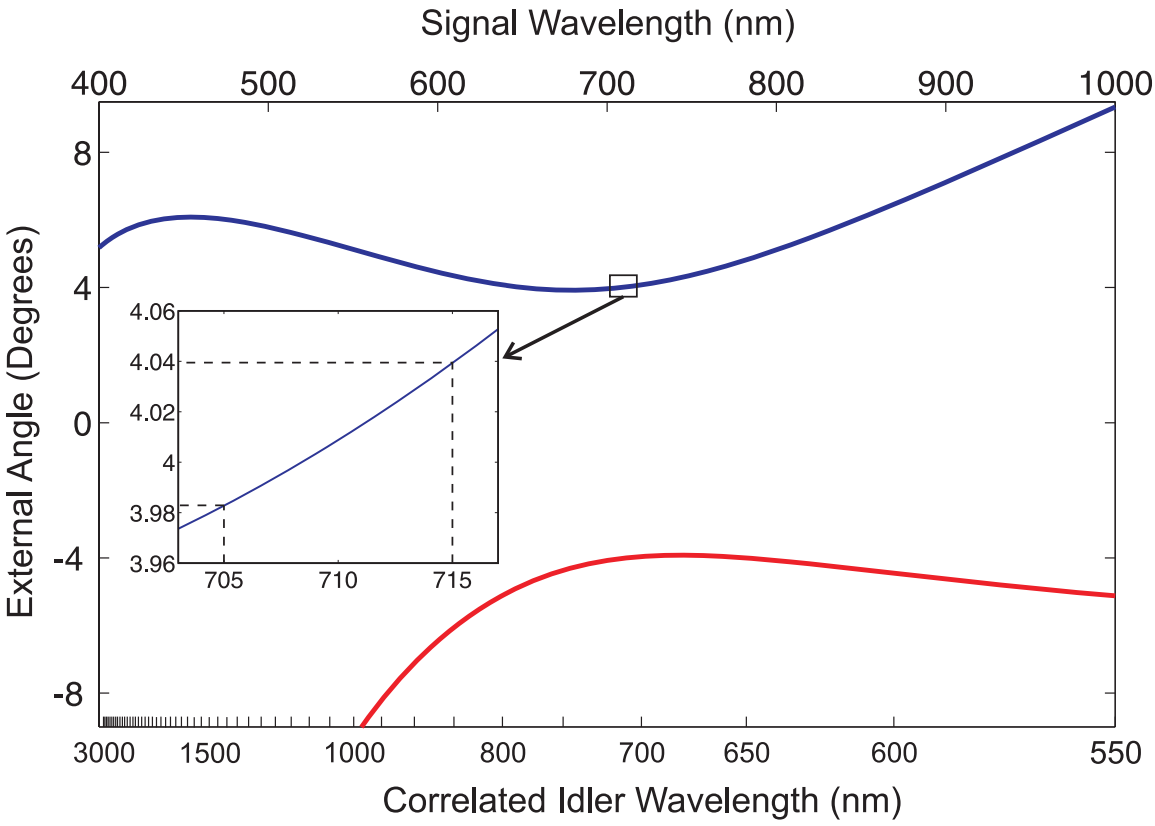

Figure 1.6 This shows the angle, from the pump, at which down converted light will come out at as a function of wavelength. 10 nm bandpass filters centered at 710 nm will admit light over an angular width of $\sim 0.06°$.

Fig. 1.6, we predict the down converted light to leave the crystal at about 4°, which is close to what we observed in the lab. Also notice that if we restrict our bandwidth by using 10 nm FWHM bandpass filters, then the acceptance angle of this band is about .06° (see the inset of Fig.1.6). If we now account for all types of spreading (see Fig. 1.5) then the acceptance angle with the band pass filters is .2°. Even when the couplers are 75 cm from the crystal an iris on the couplers will limit the viewing angle to be $\Delta\theta = .9°$. Thus, the bandpass filers will limit how much of the down conversion ring we collect.

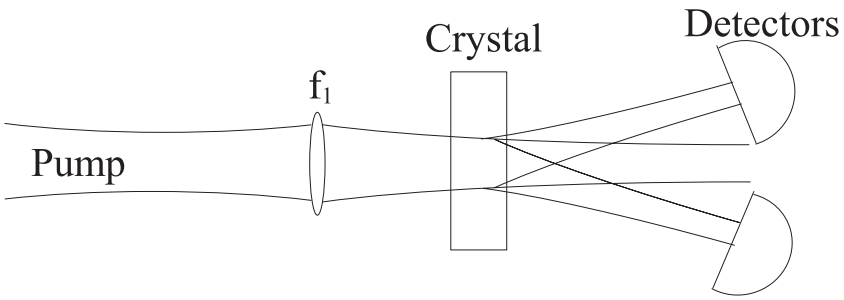

Figure 1.7 Experimental setup used by Monken el al. The pump beam is focused with a lens which causes the signal, and idler beams to focus.

1.6 Related Work

Several other groups have studied methods for customizing the output of PDC. Monken *et al.* showed the angular spectrum of the pump beam can affect the coupling of the down converted light [14]. They showed that the angular spectrum of the pump beam is mapped onto the signal and idler photons if the crystal is thin. In their experiment, they focused the pump laser to a plane after the down-conversion crystal and found that the down-converted light also focused in this plane (see Fig 1.7). They used this effect to enhance the number of photons on their detectors, which were placed at the focus plane [15] (they focused the down-converted light directly on the APD detectors rather than going through fibers). While this experiment does not couple down-converted light into fiber optics, it illustrates the ability to manipulate the geometry of the down-converted light by manipulating the pump beam.

Kurtsiefer *et al.* [16] considered a case closer to our experimental investigation. In their experiment, they collected Type II down-converted light into single-mode fibers. In Type II down-conversion, light is emitted in two offset cones. Kurtsiefer *et al.* arranged for the rings to intersect at two points, and collected light from the two intersection (this creates polarization entanglement which was important for their experiment). They focused the pump beam with a lens, and placed the focus at the

crystal (see Fig. 1.7). The focus was chosen so that the crystal length was smaller than the Rayleigh length, making the beam essentially collimated through the crystal. The lenses used to couple the light into the fibers were chosen such that the angular acceptance of the coupling system matched the angular spread of the light due to the bandwidth of their filters (different colors are emitted at different angles). With the optimized collection efficiencies of this setup, they were able to achieve significant improvements over previously reported coupling experiments. Their modeling primarily treated the phasematching as being perfect, and considered spreading due to bandwidth (i.e. different colors going different directions).

Ljunggren and Tengner [17] did a thorough study of improving collection efficiencies for Type II collinear down converted photons created by using a periodically polled KDP crystal[1] (PPKTP) and a CW laser (see Fig. 1.8). They pumped the crystal with a 532 nm laser and collected non-degenerate photon pairs at 810 nm and 1550 nm. They focused the pump with an achromat lens into the crystal. The down-converted light was focused using a second achromatic doublet lens, and the two photons were sent to the appropriate detector using a dichroic mirror. Each detector had another lens that coupled the light into a single-mode fiber.

They numerical modeled this system, and accounted for the spreading of light caused by focusing the pump beam, for imperfect phase matching, as well as for the length of the crystal. Using this setup, and their numerical model, they showed that the pump, signal, and idler waists need to be different sizes to be the most efficient. However, to get close to the most efficient one can choose all the waists to be the

[1] A periodically poled crystal, is a crystal where the orientation of the crystal axes alternates between, usually, two different values. By doing this, the crystal can be designed so the down converted light upstream does not destructively interfere with light created down stream. This is called quasi-phase matching.

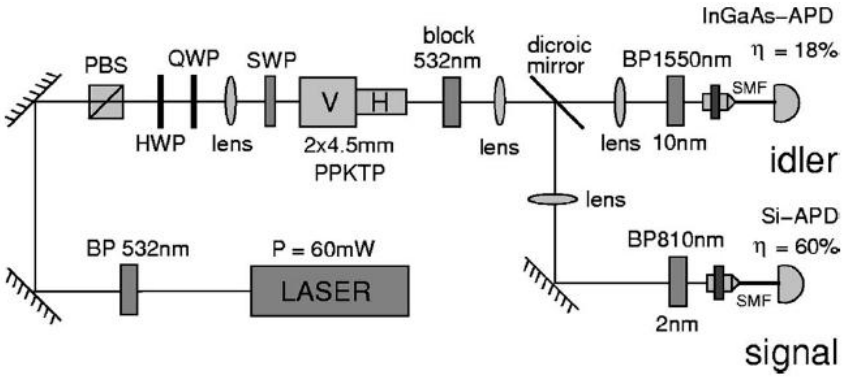

Figure 1.8 Experimental Setup used by Ljunggren, and Tengner. [17].

same size. They also claim that the waists of the pump beam, and signal and idler collection modes should be placed in the middle of the crystal, and that their Rayleigh ranges should be comparable in size to the length of the crystal L for best coupling efficiency. They also concluded that the number of down converted photons produced increases as the length of the crystal increases by the $\sqrt{L}$.

While there are similarities between the Ljunggren experiment and ours, there are several distinctions. Our experimental investigation uses Type I down conversion, and we collect degenerate photon pairs. We find that having the all the waists be the same size and at the crystal does come close to being the most efficient, but is not the most efficient. Unlike Ljunggren and Tengner we found that the longer collection modes (with a Rayleigh ranges much longer than the crystal) is desirable.

Chapter 2

Experimental Setup

In this chapter we detail the experimental setup that was used to study coupling of down-conversion. We begin in section 2.1 with an overview of Gaussian beams. In section 2.2 we go over the physical layout of the experimental system, and in section 2.3 we detail the electronic system used to record the data. Finally, in 2.4 we will go over the alignment procedures used to align the coupler.

2.1 Gaussian Beams

An important part of our experiment is the manipulation and characterization of our pump laser and collection modes. We use a simple Gaussian beam model to describe these modes. Since we will refer the Gaussian parameters frequently in our discussion, we take a moment here to briefly introduce the terminology that we use to describe Gaussian beams.

The electric field of a gaussian beam is given by [18]

$$E(\rho, z, t) = E_0 \frac{w_0}{w(z)} e^{-\frac{\rho^2}{w^2(z)}} e^{ikz + i\frac{k\rho^2}{2R(z)} - i \arctan \frac{z}{z_0}} \tag{2.1}$$

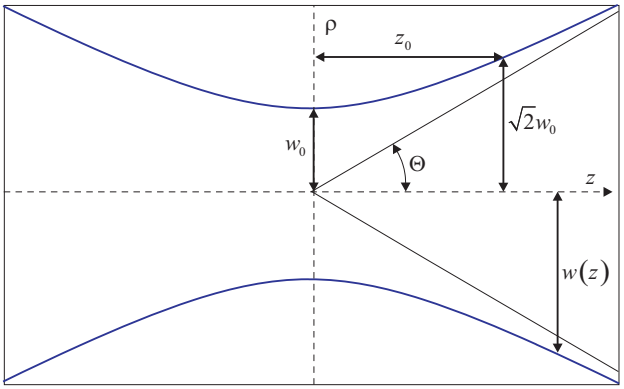

Figure 2.1 Spatial profile of a Gaussian beam.

where

$$\rho^2 \equiv x^2 + y^2 \tag{2.2}$$

$$w(z) \equiv w_0\sqrt{1 + \frac{z^2}{z_0^2}} \tag{2.3}$$

$$R(z) \equiv z + \frac{z_0^2}{z} \tag{2.4}$$

$$z_0 \equiv \frac{kw_0^2}{2}. \tag{2.5}$$

Figure 2.1 shows the $1/e$ width of the beam as it propagates along the z-axis. The cartesian coordinates x, and y axes are in the perpendicular directions, but because of the radial symmetry of the beam we typically work with the cylindrical coordinate ρ. $R(z)$ is the radius of curvature of the beam, and $w(z)$ describes the $1/e$ width of the beam as a function of propagation distance (see Fig. 2.1). The smallest width w_0 is referred to as the waist of a beam. Notice that the width of the beam asymptotes to a line at angle

$$\Theta = \frac{\lambda}{\pi w_0} \tag{2.6}$$

to the pump beam. The angle Θ is called the divergence of the beam. The Rayleigh range, z_0, is the length from the focus to the point where the $1/e$ width has grown to $\sqrt{2}w_0$.

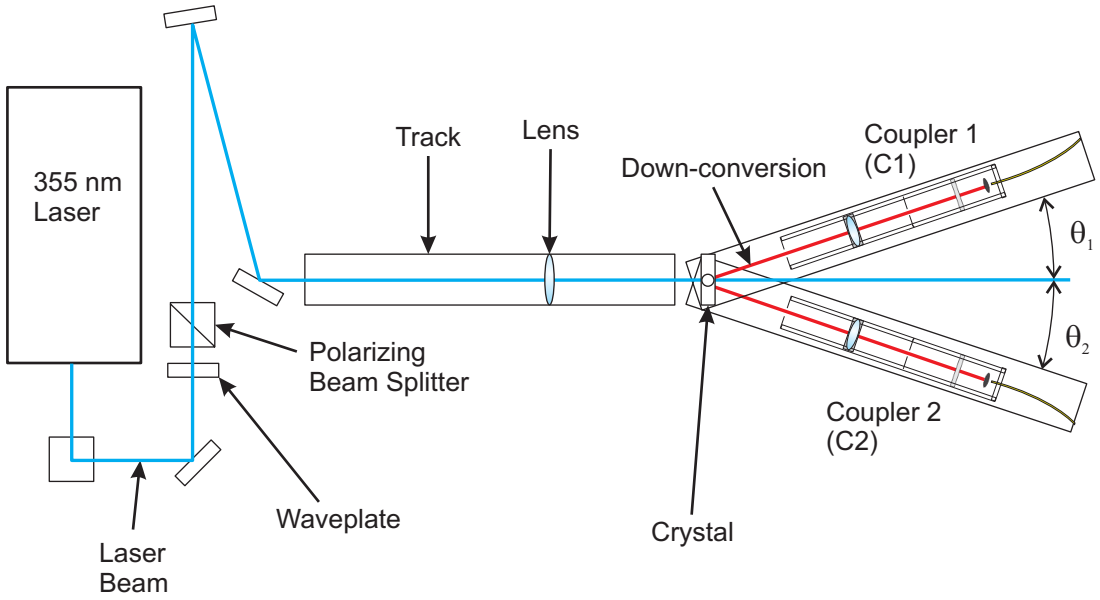

Figure 2.2 Experimental Setup. A 355 nm laser is used to pump the BBO crystal which produces the down converted photons some of which are collected by the couplers C1, and C2. A lens is placed in the pump beam before the crystal to improve collection efficiencies.

2.2 Experimental Layout

A diagram of our experimental setup is shown in Fig. 2.2. Our pump is a Coherent Paladin laser, which has a wavelength of 355 nm with pulses > 5 ps at an 80 ± 1 MHz repetition rate. At the exit of the laser head the beam has a waist of $w_0 = 0.495$ mm, $M^2 = 1.1$, and a divergence of 460 μrad. The pump beam passes through a waveplate and a polarizing beam splitter, which allows us to control the beam power. Figure 2.3 shows a CCD image of the laser beam profile, taken a little over a meter from the laser head (with no lens in the beam).

The pump beam is directed straight along a 1 m optical track before coming to the down-conversion crystal. A Lens can be mounted on the track, which allows us to focus the beam and easily adjust the distance between the lens and the crystal. The lens is mounted on a x-y translation stage so that we can ensure that the beam

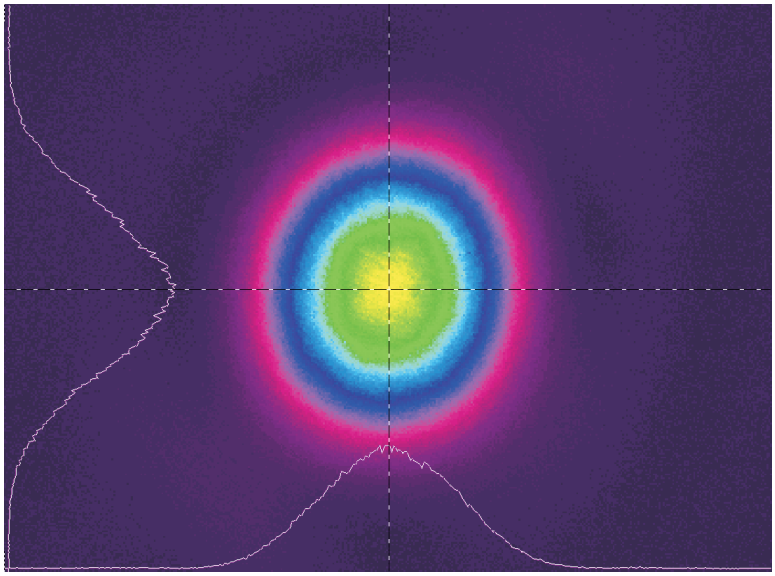

Figure 2.3 Pump beam profile, with no lens in the beam, at $d_2 = 113$ cm.

passes through the center of the lens. The pump beam then passes through a 5 mm BBO crystal, cut with the optic axis at $\theta = 33.4°$ and tilted at $0.2°$ from normal. This produces degenerate Type I down converted 710 nm photons at an angle of $\sim 4°$ from the pump beam. The residual pump beam is discarded in a beam dump.

The down-converted light is collected into single-mode fibers using the coupling system shown in Fig. 2.4. The waist can be selected by adjusting the distance between the fiber tip, and the aspheric lens[1]. An achromat lens[2] can also be attached to aid in selecting the waist. The fiber is mounted on an x-y translation stage so that it can be moved independent of the aspheric lens. Translating the fiber primarily changes the angle that the collection mode makes with the z-axis. Each coupler is mounted on an

[1]Most lenes have surfaces that are part of a sphere, and thus they have a radius of curvature. Aspheric lenes, however, have some other shape to them. They are often used to correct for spherical abberations, and are also commonly used to couple light into optical fibers.

[2]An achromatic lens is a lens that corrects for chromatic abberations. They also can be diffraction limited, and thus introduce less distortions in our beam.

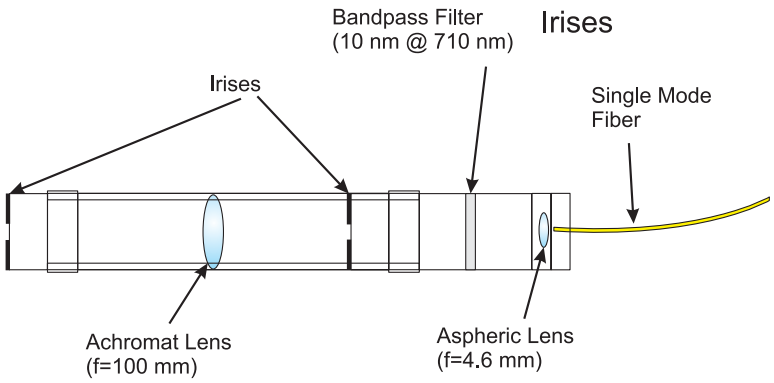

Figure 2.4 Simplified version of the couplers showing the optical components. The irises are used to align the two lenses. However the achromat lens is optional.

x-y-z translation stage and a rail, so that the waist can be placed at the crystal. The rail pivots directly beneath the crystal, allowing the angle θ, between the pump beam and the collection mode, to be coarsely adjusted (see Fig. 2.2). A 10 nm FWHM bandpass filter centered at 710 nm is placed before the aspheric lens, and the entire optical path from the filter to the fiber is surrounded by a light-tight enclosure to eliminate background light. Irises are installed to help align the lens(es).

Fig. 2.5 defines some distances. The most important one, d_{2p}, is the distance between the lens and the middle of the crystal. The pump beam lens could be a variety of lens placed a distance d_{2p} from the middle of the crystal. Table 2.1 shows common pump lenses with focal length f_p which produce a waist w_{0p} at the crystal ($d_{3p} = 0$).

We could view the collection modes by coupling a 710 nm laser into a single mode fiber attached to a coupler. Then a beam profiler CCD camera can view the beam so that we can select w_{0c}, and d_{3c} (or d_{2c} depending on whether a collection lens is present).

$w_{0c} = 350$ μm was produced ~ 60 cm from the coupling lens, when the collection lens on the couplers was removed. For $w_{0c} = 225$ μm and 105 μm the collection

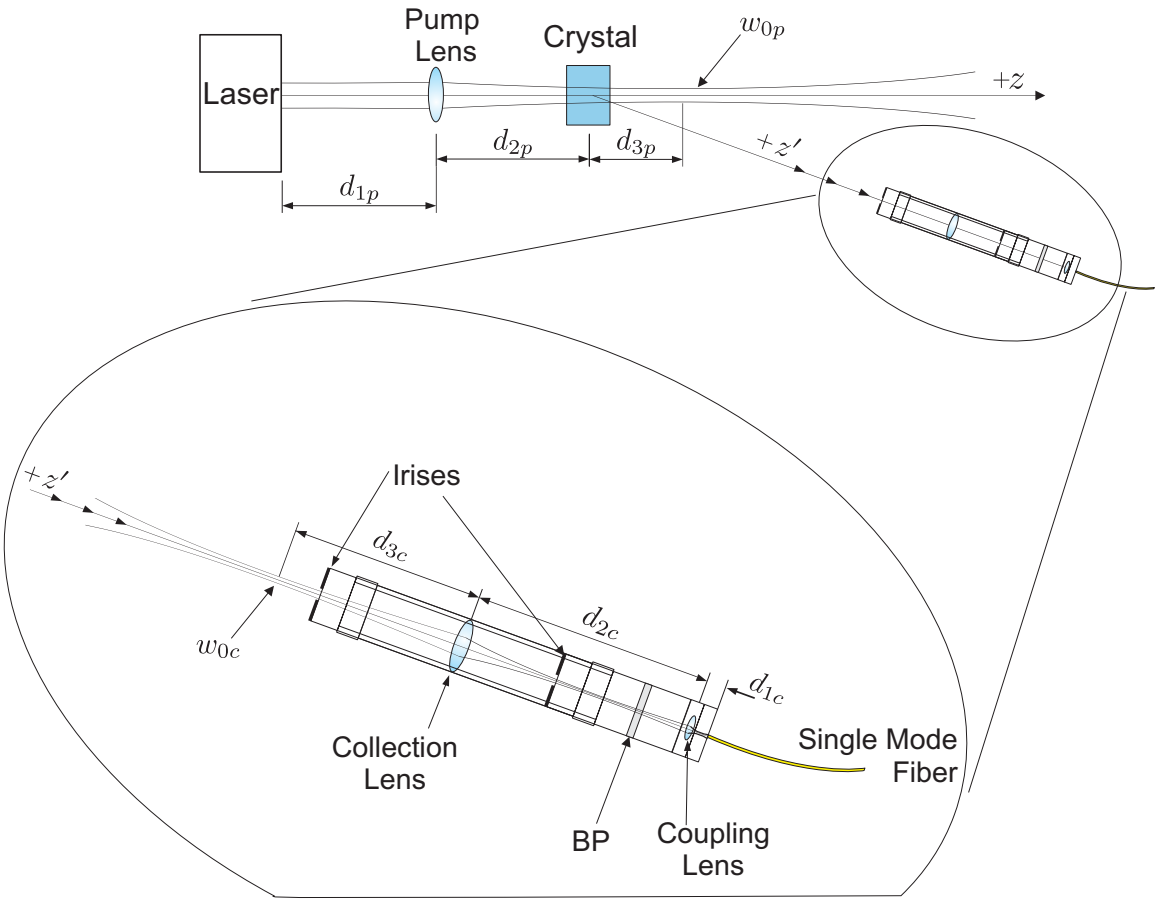

Figure 2.5 A simplified view showing the pump beam and collection modes, as well as relevant distances. Since the path of the down converted light to each coupler is symmetric only one coupler is shown. BP is the bandpass filler, and d_{2p} and d_{3p} are measured from the center of the crystal. w_{0p} and w_{0c} are the pump waist and collection waist respectively.

lens was in the couplers, which produced the waists at $d_{3c} = 59$ cm, and 36 cm, respectively.

2.3 Electronics

The down-converted light collected by the fibers is coupled into single-photon counting modules (Perkin-Elmer SPCM-AQR-14-FC). These modules are avalanche photodiode (APD) based detectors. When the detection modules sense photons, they send

f_p (cm)	d_{2p} (cm)	w_{0p} (μm)
20	21	37
30	34.5	70
50	51.5	185
75	59.5	265
100	71.5	355

Table 2.1 This table shows the measured waist at the crystal when f_p is placed in the pump beam at a distance d_{p2} from the crystal.

logic-level signals to a high speed time-digitizing board (Ortec 9353). The two inputs to this digitizing board are referred to as the "start" channel and the "stop" channel. The signals on the start channel act as a trigger that tells the board to start a scan that records the arrival time of each subsequent stop signal for .2 μs (with a precision of 100 ps). The computer records the total number of start and stop signals that are received during a specified gate pulse (1 sec long) which allows us to find the rate of the start s_{starts}, and stop counts s_{stops} (counts per second). The computer also produces a cumulative histogram (see Fig. 2.6) of the delays between the arrival of start and stop pulses. Since, the optical path of the twin photons is nearly the same, we would expect them to hit the detectors at about the same time. Thus, the stop channel signal is delayed (using a longer cable) to allow the computer some time to begin a scan. As a result the stop pulses should come in at a specific time (between 12-20 ns) if the detectors were triggered by down converted photons.

If stop pulses come in at different times we assume it is caused by stray light from the background. When we calculate coincidence counts C_c (counts per second) we subtract off the background by counting the number of stop counts between 29-37 ns(this catches one of the peaks shown in Fig. 2.6), and subtract this off from

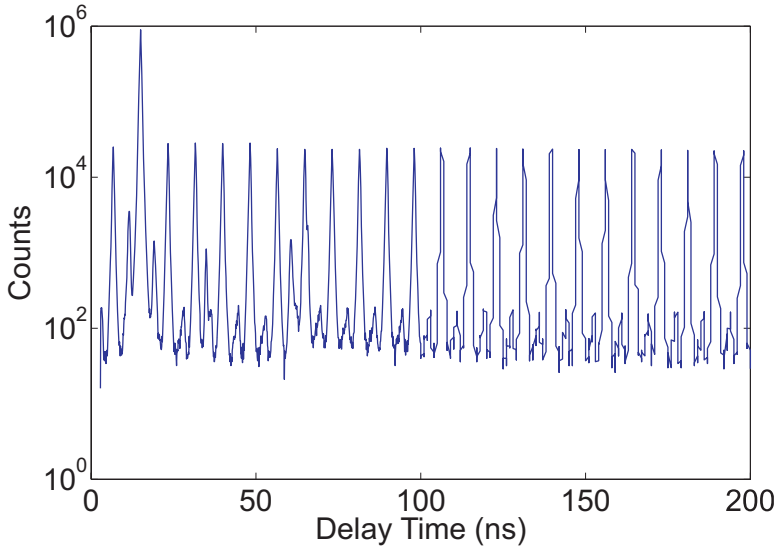

Figure 2.6 Plot of the time (in ns) when "stop" pulses arrive at the computer. The largest spike from 12-20 ns is the coincidence pulses. The other spikes are a result of the laser being pulsed.

the counts that arrived between 12-20 ns. From the $s_{\text{starts,stops}}$, and C_c we can also calculate the efficiency by

$$E = \frac{C_{\text{c}}}{(s_{\text{stops}} + s_{\text{starts}})/2}. \tag{2.7}$$

The computer stores data on the rates $s_{\text{starts,stops}}$, C_c, and E in a file every second the computer is taking data. When it comes time to analyzing the data we average over all the data stored in the file to find the average $s_{\text{starts,stops}}$, C_c, and E. Then the results are plotted in figures such as Figs.3.1,-3.4.

2.4 Alignment Procedure

There are two types of alignment procedures that we used. The first one (Type A) is done by aligning detector C2 (see Fig. 2.2) to maximize singles counts, and the other detector (C1) to maximize coincidence counts. If a lens has to be placed in the pump

beam then the lens is placed in the beam first so that the beam follows the original path of the laser beams. After this the detectors are aligned.

The other alignment procedure (Type B) that we used is to align the detectors by maximizing both detectors to the singles counts, and then we moved them around until the efficiency is maximized. After that a lens may be placed in the beam, and translated in directions perpendicular to the beam until the detectors are at maximum efficiency.

Once the detectors are aligned sufficiently to get coincidence counts the latter method takes more time ($\sim$ 2 hours), while the other is faster ($<$ 30min.). To see if the alignment procedures come to the same result we used the same configuration (350 μm collection waist at the crystal, and no lens in the pump beam) each time we aligned. The Type A alignment procedure produced an efficiency of 11.6%, while Type B gave an efficiency of 11.9%. Thus, Type B did a little bit better in efficiency, but at the expense of time. This doesn't seem too surprising because there are many of degrees of freedom, and varying them in different ways could result in converging to different maximums.

Chapter 3

Measurements

We used our apparatus to explore the effect of pump laser and collection mode focusing on collecting both single photons and photon pairs by preforming two main experiments. In Experiment I we placed the pump and collection waists at the crystal and varied w_{0p} and w_{0c} to see what configuration yields the best count rates and coupling efficiencies. In experiment II we moved the pump lens, so that the pump waist went from before the crystal to after the crystal. We also characterized the effects of waist placement on efficiency in Experiment III.

3.1 Experiment I

Single Count Rates

Our first experiment characterized the dependence of singles counting rates (the rate at which photons are detected with one detector without regard for the other) on w_{0p} and w_{0c}. Figures 3.1 and 3.2 show data obtained in this measurement. In this setup, the lenses on the couplers were arranged to place the collection mode waist at the crystal, and were left fixed for each data set (a, b, and c). The pump beam was then

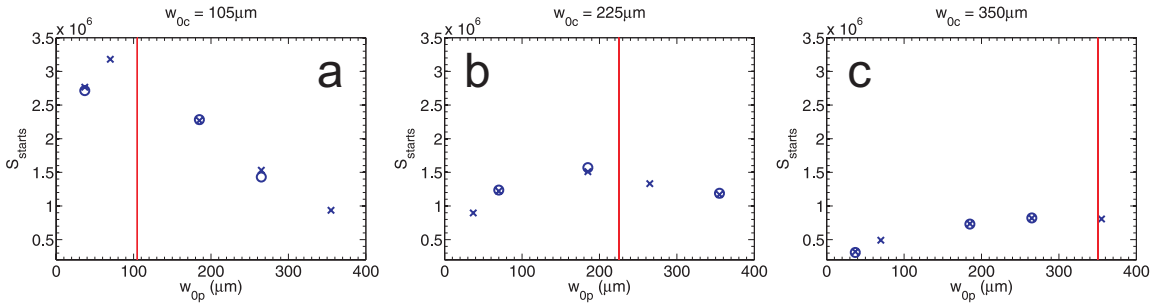

Figure 3.1 Plot of single counts vs. w_{0p} on the start channel (C2) for different collection waists. The vertical line in each plot represents the waist of the collection modes.

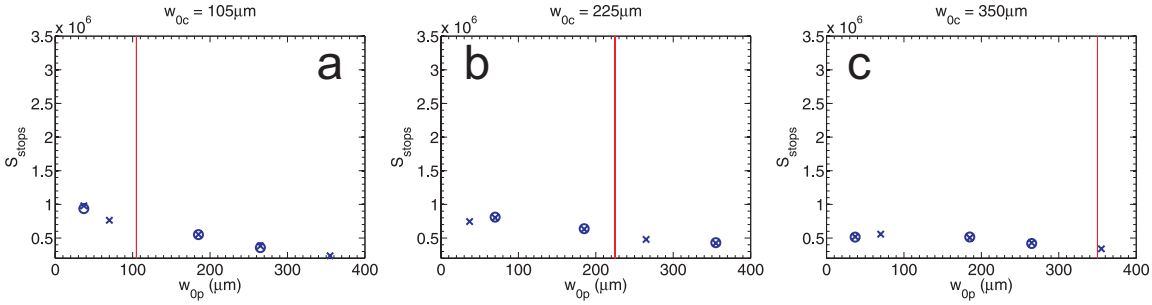

Figure 3.2 Plots of singles counts vs. w_{0p} on the stop channel (C1) for a specified collection mode w_{0c}. The vertical line in each plot represents the waist of the collection modes.

focused at the crystal ($d_{3p} = 0$) and w_{0p} was changed by swapping in pump lenses of varying focal lengths. We positioned the couplers so that the track they ride on makes an angle of $\sim 4 - 5°$ with the pump beam, and then aligned them using the Type A alignment procedure. After the optics were aligned, the data was recorded. This procedure was repeated for three different collection modes and the results are plotted in the different frames. The x data points indicate data from the first series, and the o data points indicate data that was taken a second time to test repeatability.

In Fig. 3.1a the collection mode was set to have a waist of $w_{0c} = 105$ μm. As w_{0p} was varied, we saw that the single counting rates were best when $w_{0p} = 75$ μm, which is similar in size to the w_{0c}. Unfortunately, we could only take a few data points

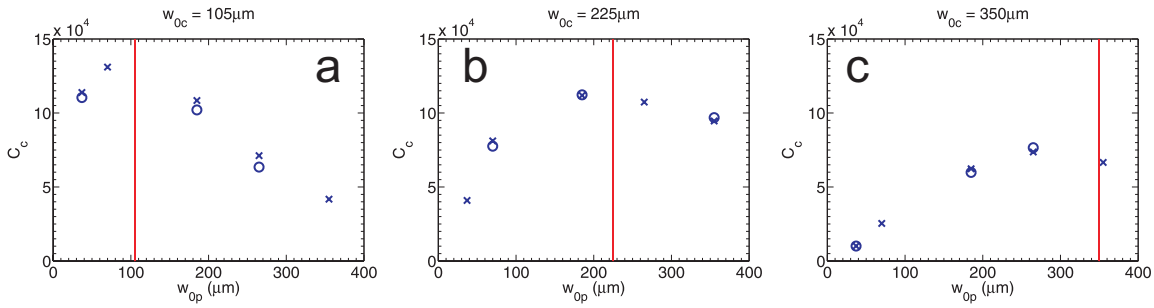

Figure 3.3 Plots of C_c vs. w_{0p} for a specified collection w_{0c}. The vertical lines in each plot represents the waist of the collection modes.

because of our finite number of pump focusing lenses. In Fig. 3.1b the collection waist w_{0c} was set at $w_{0c} = 225$ μm, and the peak occurs when the pump waist was $w_{0p} = 185$ μm. In Fig. 3.1c the collection waist was set to $w_{0c} = 350$ μm, and this time we see the singles counts leveling off, or with a peak at $w_{0p} = 265$ μm.

Coincidence Count Rates

Figure 3.3 shows how the coincidence counts change as w_{0p} varies, and $d_{3p} = 0$. This data was taken at the same time the single count rate data was taken. Once again some of the points were taken twice to get a feel for the amount of error in our measurements. The differences were $< 11\%$.

From the data in Fig. 3.3, we see a similar trend as we did for the singles counts in the previous subsection. Once again the coincidence counts are at a maximum when the pump waist at the crystal is of comparable size to the collection mode waist.

Collection Efficiency

Fig. 3.4 shows how the efficiency changes as w_{0p} and w_{0c} change. Plot A in Fig. 3.4 corresponds to a w_{0c} of 105 μm and has a maximum efficiency of 7.7% when w_{0p} is 185 μm. Plot B has a w_{0c} of 225 μm and the maximum of 12% occurs when the w_{0p}

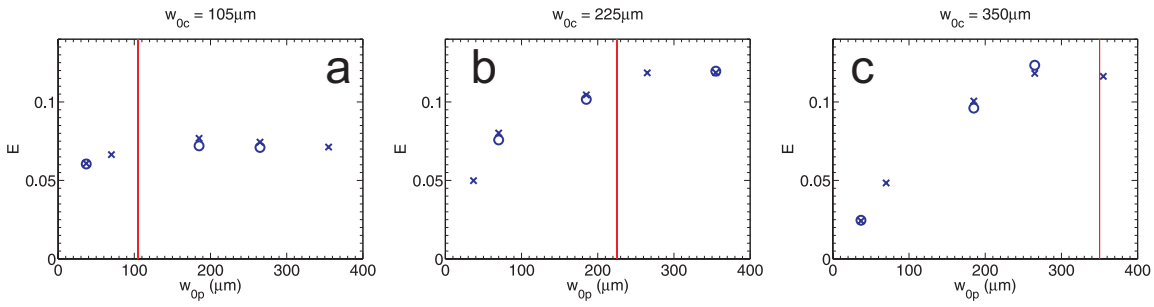

Figure 3.4 The efficiency changes as the pump w_{0p} and collection w_{0c} change. Once again the vertical line represents the collection w_{0c}.

is 355 μm. Finally, plot C in Fig. 3.4 has a w_{0c} of 350 μm and a maximum efficiency of 12.3% when w_{0p} is 265 μm. Also the variation between the first and second sets of data is $< 7\%$.

In the Figs. 3.4a and 3.4b there appears to be a leveling off or slight decline at larger pump mode sizes. However, like the singles counts we cannot really tell if the efficiency asymptotes or comes to a peak and then declines. We conclude that the collection waist and pump waist are nearly the same when the efficiency is maximized. This agrees with Ljunggren and Tengner who concluded that having all the waists the same size and at the crystal is not the most efficient, but is close to the most efficient.

Collection Mode

Fig. 3.5 presents the highest efficiencies in Figs. 3.4a-c with the corresponding start counts. Each of these is plotted against w_{0c}. As the collection modes become larger the efficiency also grows, but the singles counts go down. Thus, showing that there is a trade off between the singles counts, and the efficiency.

Also the 350 μm collection mode is significantly more efficient than any of the measurements made with the 105 μm collection mode. In our experiment the Rayleigh

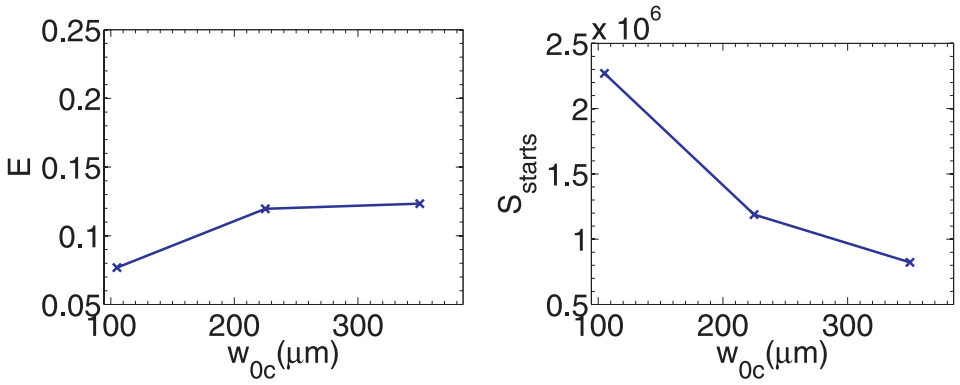

Figure 3.5 The highest efficiency in Figs.3.4a-c are plotted vs. the collection waist. Also the corresponding start counts are plotted vs. the collection waist.

length for the 350 μm collection mode is $\sim$ 1.1 m, and the length of the crystal is about 5 mm. This means that the more efficient configurations have Rayleigh lengths much larger than the length of the crystal. This is different from what Ljunggren and Tengner [17] observed, which is the Rayleigh length of the collection mode should be about 2-3 times the length of the crystal for the most efficient configuration.

3.2 Experiment II

Single Count Rates

In a second experiment we moved the pump lens so that the location of the pump waist (d_{3p}) changes, while the collection modes are held constant for each data set. The couplers were aligned using the Type B alignment procedure. After the optics were aligned the data was recorded. The data for this experiment are presented in Figs. 3.6-3.8

Surrounding the main figure are several small figures that indicate the relative size and positions of the pump and collection modes. Each plot was made by measuring

the waist of a given mode (either collection or pump mode) using a CCD camera and the location of the waist from the crystal. The mode was then plotted assuming a Gaussian profile (described in chapter 2.1) with the measured waist size and position. Some data points don't have plots, because the CCD camera could not easily get to the waist of the beam to measure it. The data used to make these plots was measured at a different time from the data shown in table 2.1, and shows slight discrepancies. The vertical line at $z = 0$ in the mode plots is actually two lines that represent the front and back of the crystal. (Since the crystal is only 5 mm long the two lines appear to be one.)

In Fig. 3.6 the coupling waist was set to $\omega_{0c} = 105$ μm. The pump laser was focused using the 30 cm lens, which produces a waist of about $w_{0p} \approx 75$ μm. The maximum for the start count rate occurs when the pump beam is focused slightly before the crystal ($d_{2p} = 40$ cm). The stop count rate is maximum when the pump is focused essentially at the crystal ($d_{2p} = 35$ cm). The Rayleigh range for the pump is $z_0 \approx 5$ cm, so we conclude that the singles counting rates are optimized when the pump focus is near (within a Rayleigh range) the crystal.

In Fig. 3.7 the pump lens was changed to have a focal length of 100 cm, which produced a pump waist of $w_{0p} \approx 355$ μm. The collection mode was set at $\omega_{0c} = 105$ μm, just as in Fig. 3.6. Thus there was a significant difference between the pump and collection modes in this setup. The the Rayleigh range for the pump is $z_0 \approx 1$ m, so we were unable to move the waist position by a significant fraction of its Rayleigh range. In this case, we see no clear maximum as the waist position is scanned.

In Fig. 3.8 we again used the 100 cm focal-length pump lens, but modified the collection mode to have a waist of $w_{0c} \approx 350$ μm. In this case, there is a clear maximum as the collection waist position is scanned (near $d_{2p} = 77$ cm).

From this data we conclude that the singles counts are maximized when the pump

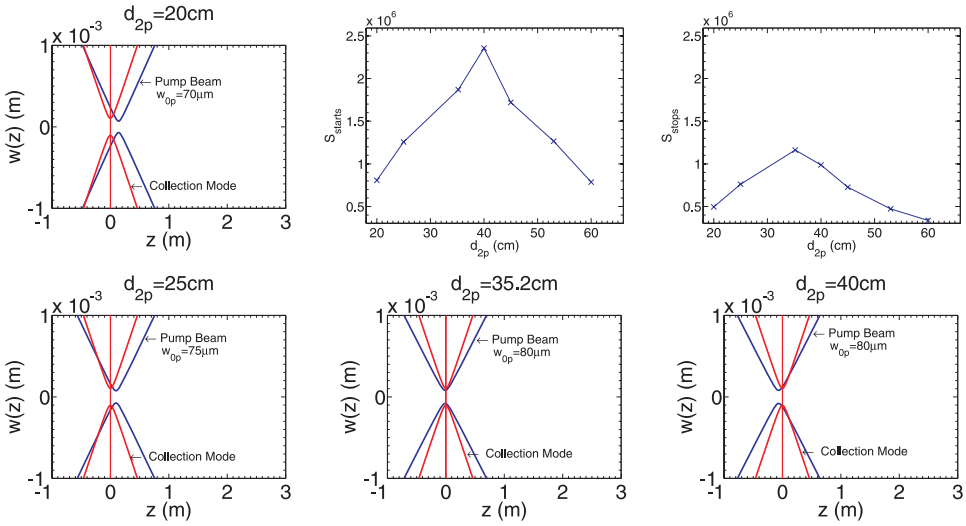

Figure 3.6 Plot of the singles count rate as the pump mode waist and position are varied (upper two on right). In this figure there are 4 plots of the collection, and pump modes (viewed from the side), and 2 data plots (upper two on right). In the mode plots, the vertical lines are placed at the front and back of the crystal. However the lines are only 5 mm apart so they may appear as one line. This figure corresponds to a collection waist of 105 μm and a 30 cm focal length pump lens.

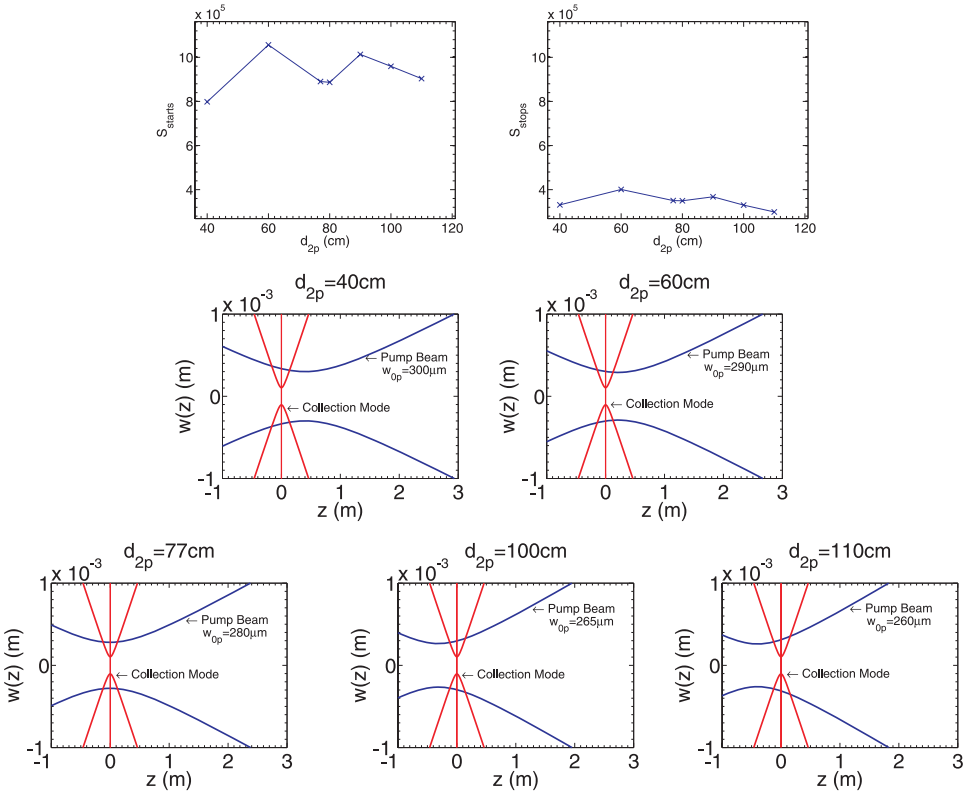

Figure 3.7 Plot of the singles count rate as the pump mode waist and position are varied. This figure corresponds to a collection waist of 105 μm and a 100 cm focal length lens in the pump beam.

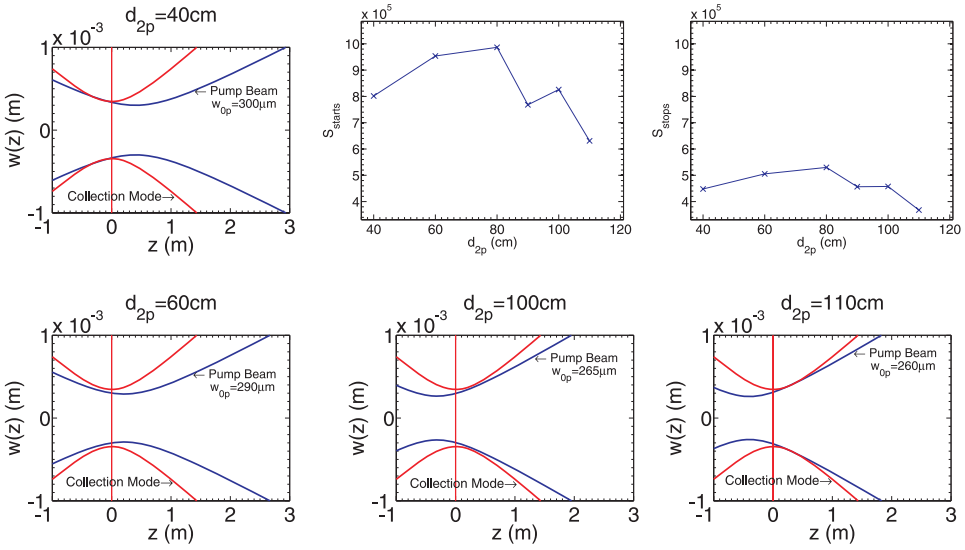

Figure 3.8 Plot of the singles count rate as the pump mode waist and position are varied. This figure is for a collection waist of 350 μm and a 100 cm focal length lens placed in the pump beam.

waist is located near the collection waist (when both waists are at the crystal). When the collection mode has an angular acceptance that is larger than the angular spread of the pump mode (i.e. the collection mode waist is smaller than the pump mode waist), as is the case in Fig. 3.8, then the singles collection is not as sensitive to the exact position of the pump waist. However, when the collection mode has a similar angular acceptance to the angular spread of the pump (i.e. when the pump and collection waists are of similar size), the relative positioning is more critical.

Coincidence Count Rates

Figs. 3.9-3.11 were obtained in the same experiment as Figs. 3.6-3.8 were in the previous subsection. Just as with the single counts, the coincidence counts are maximized when the pump waist is near the crystal. This is expected since greater single counting rates will naturally lead to higher coincidence rates. What is perhaps more interesting is how the collection efficiency is affected by the varying waist sizes.

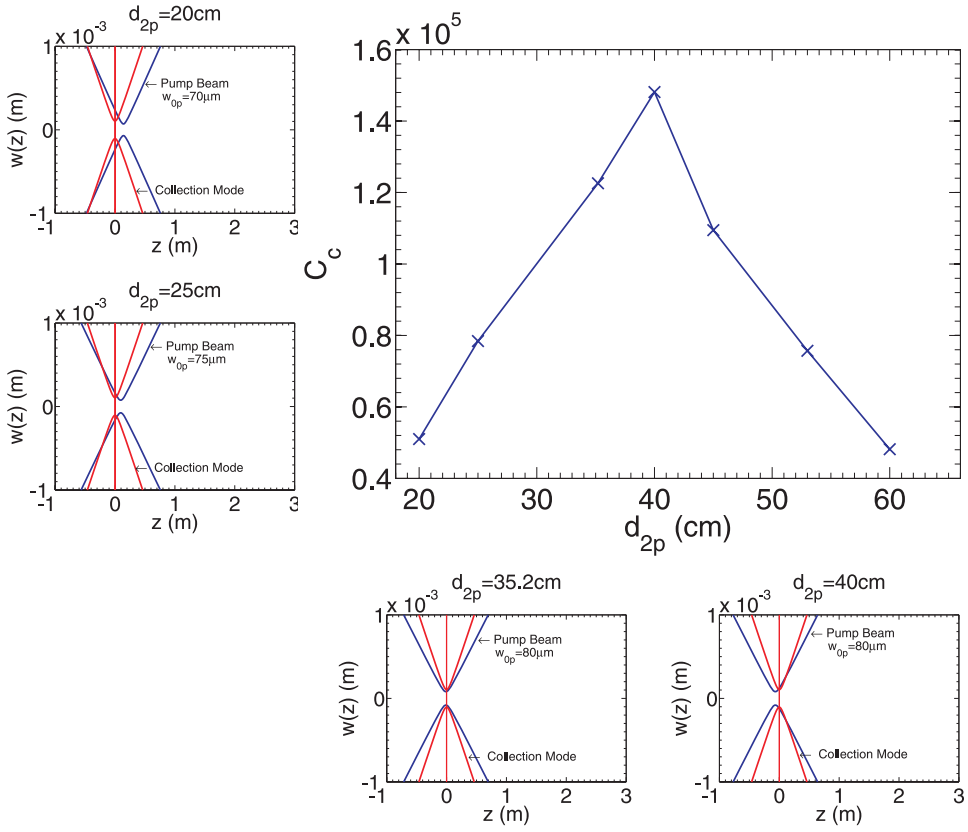

Figure 3.9 Plot of the coincidence count rate as the pump mode waist and position are varied. This figure corresponds to a collection waist of 105 μm and a 30 cm focal length pump lens.

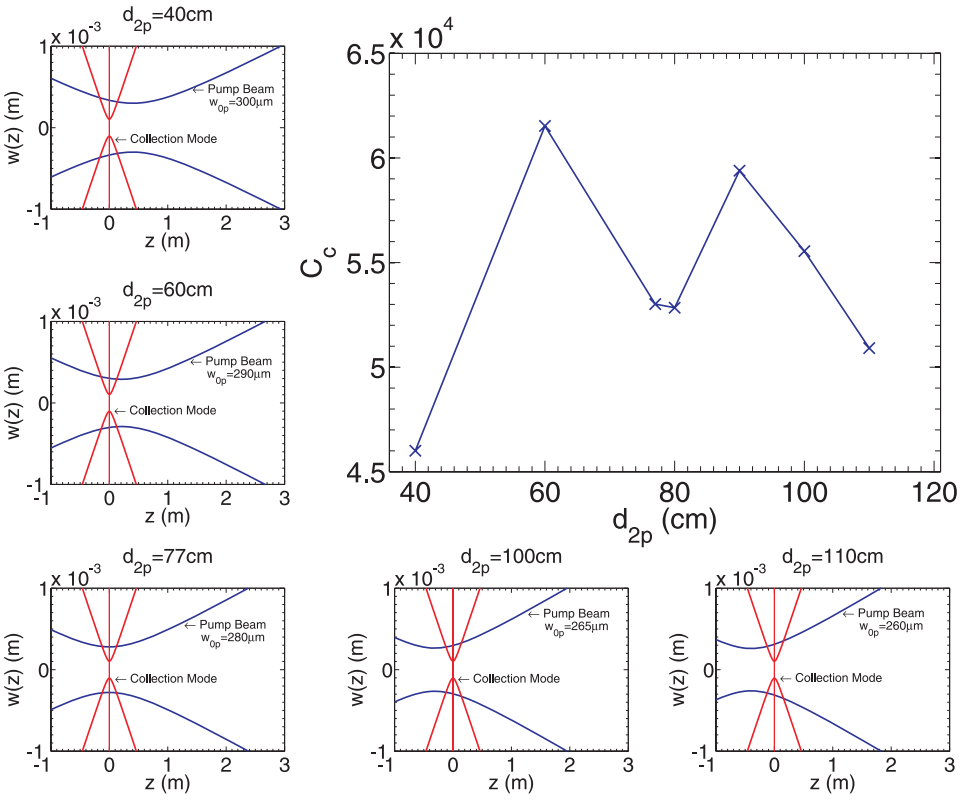

Figure 3.10 Plot of the coincidence count rate as the pump mode waist and position are varied. This figure corresponds to a collection waist of 105 μm and a 100 cm focal length lens in the pump beam.

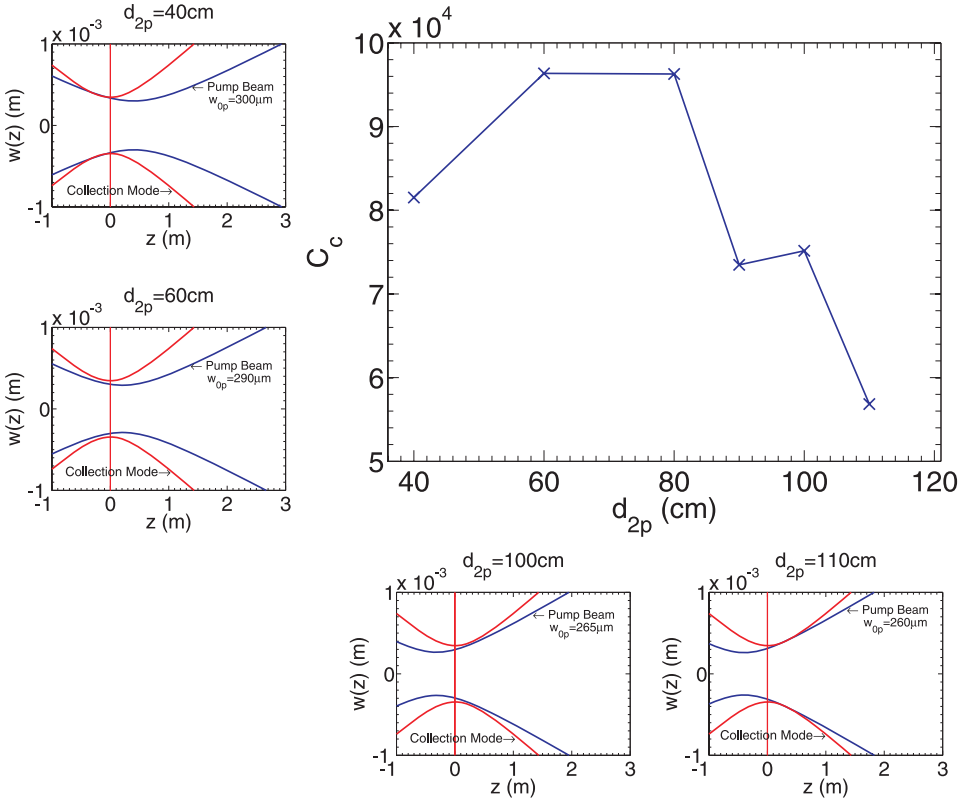

Figure 3.11 Plot of the coincidence count rate as the pump mode waist and position are varied. This figure is for a collection waist of 350 μm and a 100 cm focal length lens placed in the pump beam.

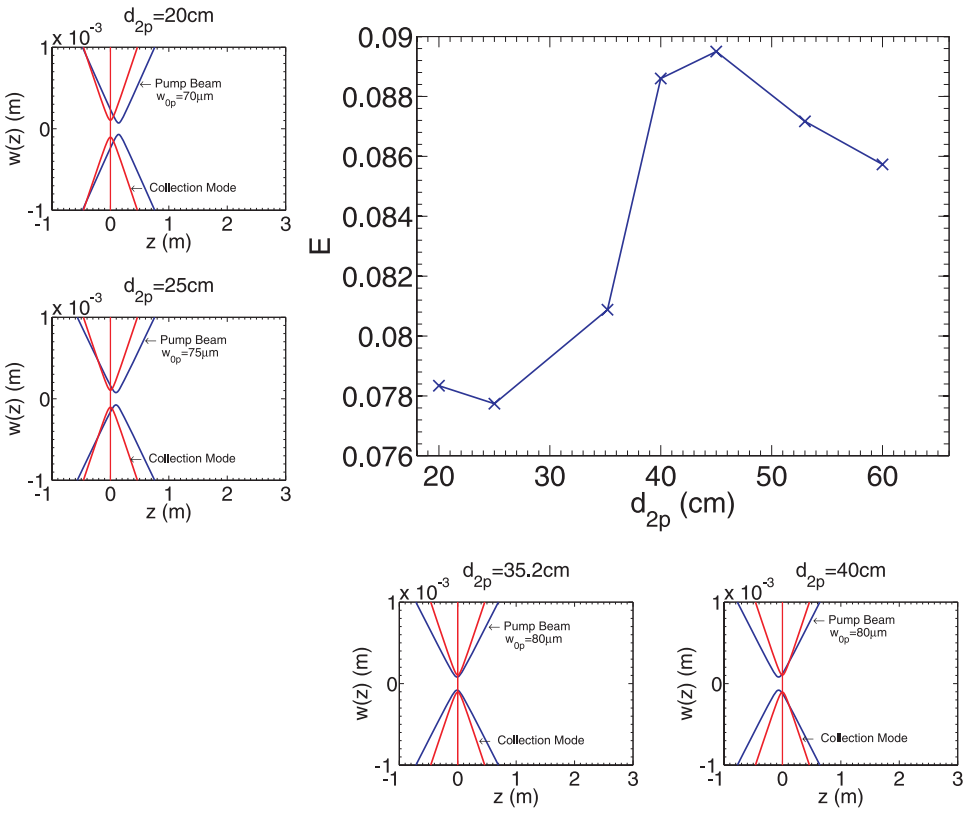

Figure 3.12 Plot of the efficiency as the pump mode waist and position are varied. The collection waist is 105 μm, and the pump waists are produced by placing a 30 cm focal length lens in the pump beam.

Collection Efficiency

The singles and coincidence counts seem to change together, and have a maximum when the waists are at or near the crystal. The efficiency (defined in sec. 2.3) also peaks when the pump waist is near the crystal.

By comparing efficiency data in figures 3.12-3.13 there seems to be little change in the efficiency (at most 2%) as the focus is moved. The position of the pump beam waist relative to the collection waist seems to play a smaller role in determining the collection efficiency than the waist sizes.

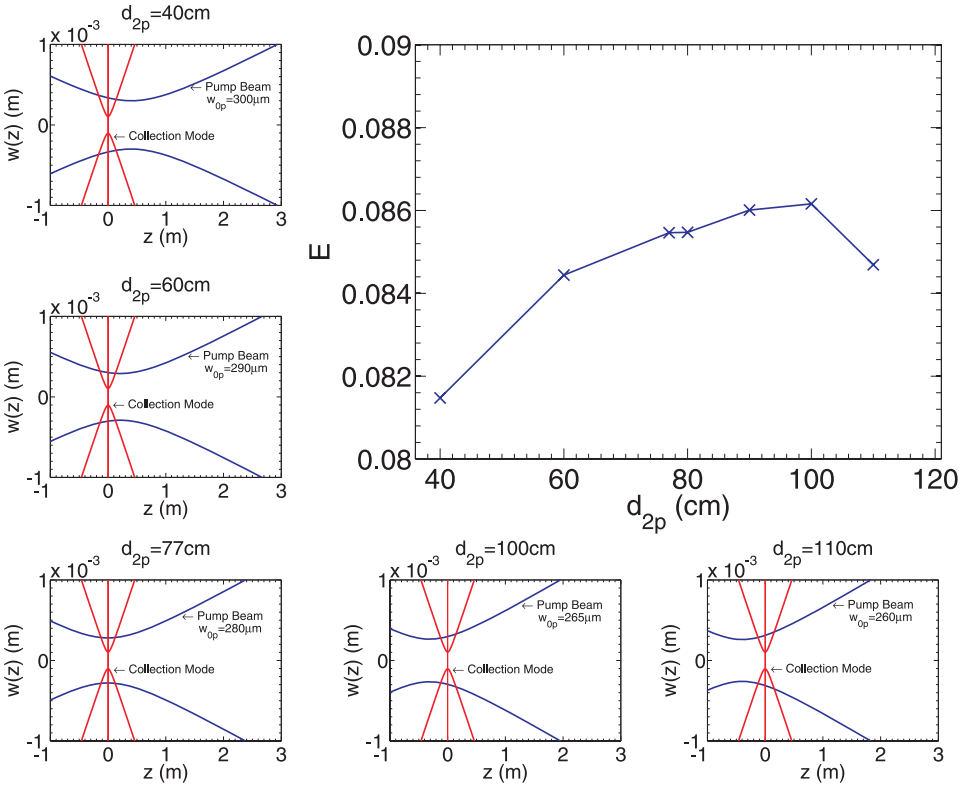

Figure 3.13 Plot of the efficiency as the pump mode waist and position are varied. This figure is for a collection waist of 105 μm and a 100 cm focal length lens placed in the pump beam.

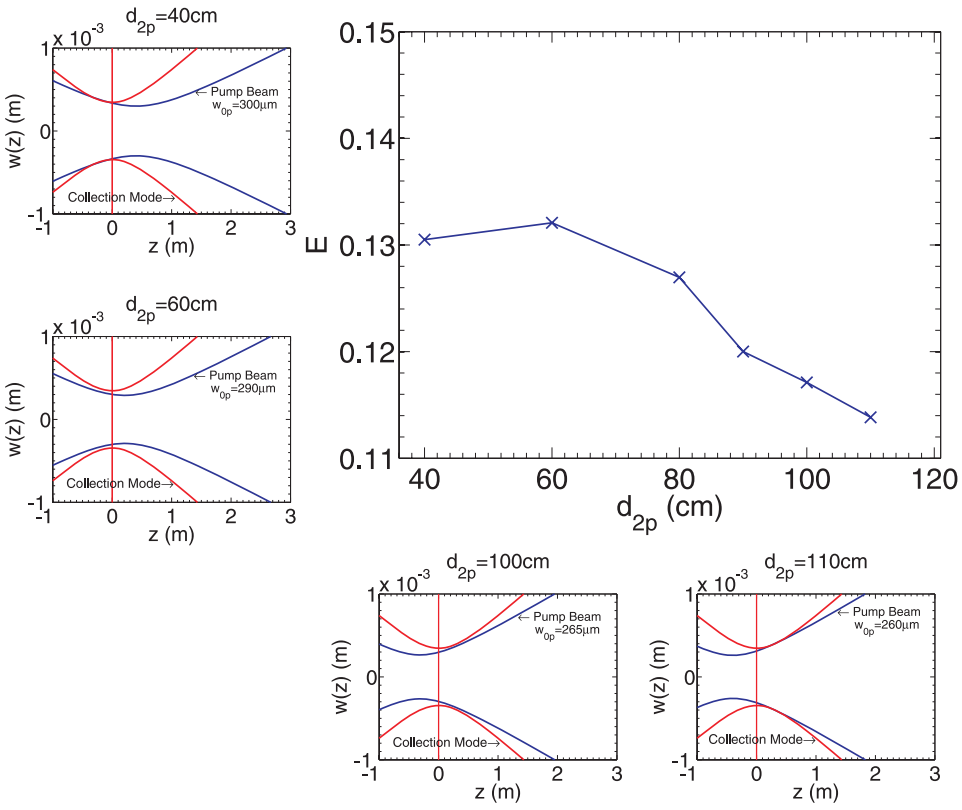

Figure 3.14 Plot of the efficiency as the pump mode waist and position are varied. This figure corresponds to a collection waist of 350 μm and a 100 cm focal length lens in the pump beam.

3.3 Experiment III-Efficiency

We also wanted to see if placing the waists at some point other than at the crystal would be better. We positioned the waists of the pump beam and the collection modes 23 cm past the crystal on the side of the collectors. The collection waists were set at $w_{0c} = 225$ μm, and the overall distance from the collectors to the crystal was 75 cm. The pump beam had a 100 cm lens which made a waist of 315 μm, 23 cm beyond the crystal. These couplers were aligned using the Type A method. The resultant efficiency was 9.0%. When all the waists were at the crystal, the efficiency was 12%. Thus, having all the waists at the crystal might be the better than having all the waists located at some other position.

With no lens in the pump beam we changed the distance between the single mode fiber and the coupling lens. This caused the collection mode waist and position to change. We found that having the collection waist near the crystal is more efficient than having it somewhere else. This is similar to the results obtained by moving a lens back and forth in the pump beam.

Chapter 4

Conclusions

In this study we used Type I degenerate parametric down conversion. We used the setup shown in Fig. 2.2 to explore the effect that the pump beam waist and position, and collection mode waist and position have on the collection efficiencies. We found that the singles counts, coincidence counts, and efficiency are best when the waists are near the crystal, and about the same size. Putting all the waists at the crystal, and making them the same size gets one close to the most efficient, which is consistent with the work of Ljunggren and Tengner [17].

In our study we were able to get collection efficiencies as high as 13.3%. In comparison Ljunggren and Tengner reported an efficiency of 11% [17] for Type II collinear down-conversion, and Kurtsiefer *et al.* reported an efficiency of 28.6% [16] for non-collinear Type II down-conversion. While the methods for computing collection efficiency are not exactly the same in each of these experiments, we can see that we are on par with these other groups.

We found that the Rayleigh range of the pump and collection mode should be much larger than the length of the crystal for the greater efficiency. However, the singles counts will go down as the collection waist becomes larger. In contrast, Ljunggren and

Tengner [17] predict that the best results are obtained when the Rayleigh length and crystal length are close to the same size. They used a somewhat different collection geometry which could account for this difference.

Methods of alignment seem to have a small effect on the maximum efficiency that one will see. The fastest method of aligning the couplers that we found is to maximize the singles counts on one coupler and then maximize the coincidence on the other coupler. To use the other method the singles counts on each detector are maximized and then efficiency is maximized by moving both detectors. This takes more time but results in slightly higher efficiencies.

In summary, good coupling efficiencies can be obtained by putting all the waists at the crystal, using relatively large collection waists, and make the pump waist about the same size as the collection waist. This procedure gives reasonably good efficiencies. While numerically modeling the system (as Ljunggren and Tengner [17] did) could give more insight into the system, the fact that we are getting similar efficiencies suggests that there are probably not huge gains to be made by varying the parameter space that we explored (pump and collection mode size and position).

Bibliography

[1] Serway, Moses, and Moyer, *Modern Physics*, 2nd ed. ed. (Harcourt College Publishers, Fort Worth, 1997), p. 68.

[2] J. L. O'Brien, G. Pryde, A. White, T. Ralph, and D. Branning, "Demonstration of an all-optical quantum controlled-NOT gate," Nature **26,** 264–267 (2003).

[3] E. Schillinger, "Money changes hands in key bank transaction," News@Nature **428,** 883 (2004).

[4] E. Klarreich, "Quantum cryptography: Can you keep a secret?," Nature **418,** 270–272 (2002).

[5] D. Boschi, S. Branca, F. De Martini, L. Hardy, and S. Popescu, "Experimental Realization of Teleporting an Unknown Pure Quantum State via Dual Classical and Einstein-Podolsky-Rosen Channels," Phys. Rev. Lett. **80,** 1121–1125 (1998).

[6] C. H. Bennett and G. Brassard, "Quantum cryptography: Public key distribution and coin tossing," Proceedings of IEEE International Conference on Computers, Systems, and Signal Processing pp. 175–179 (1984).

[7] L. K. Grover, "A fast quantum mechanical algorithm for database search," Proceedings, 28th Annual ACM Symposium on the Theory of Computing (STOC) pp. 212–219 (1996).

[8] C. Santori, M. Pelton, G. Solomon, Y. Dale, and Y. Yamamoto, "Triggered Single Photons from a Quantum Dot," Phys. Rev. Lett. **86,** 1502–1505 (2001).

[9] A. Aspect, J. Dalibard, and G. Roger, "Experimental Test of Bell's Inequalities Using Time- Varying Analyzers," Phys. Rev. Lett. **49,** 1804–1807 (1982).

[10] A. Einstein, B. Podolsky, and N. Rosen, "Can Quantum-Mechanical Description of Physical Reality Be Considered Complete?," Phys. Rev. **47,** 777–780 (1935).

[11] A. L. Migdall, D. Branning, and S. Castelletto, "Tailoring single-photon and multiphoton probabilities of a single-photon on-demand source," Phys. Rev. A **66,** 053805 (2002).

[12] N. Boeuf, D. Branning, I. Chaperot, E. Dauler, S. Guerin, G. Jaeger, A. Muller, and A. Migdall, "Calculating Characteristics of Noncollinear Phase Matching in Uniaxial and Biaxial Crystals," Opt. Eng. **39,** 1016–1024 (2000).

[13] M. Ware and A. L. Migdall, "Single-photon Detector Characterization Using Correlated Photons: the March from Feasibility to Metrology," J. Mod. Opt. **15,** 1549–1557 (2004).

[14] C. H. Monken, P. H. S. Ribeiro, and S. Padua, "Transfer of angular spectrum and image formation in spontaneous parametric down-conversion," Phys. Rev. A **57,** 3123 (1998).

[15] C. H. Monken, P. H. S. Ribeiro, and S. Padua, "Optimizing the photon pair collection efficiency: A step toward a loophole-free Bells inequalities experiment," Phys. Rev. A **57,** R2267 (1998).

[16] C. Kurtsiefer, M. Oberparleiter, and H. Weinfurter, "High-efficiency entangled photon pair collection in type-II parametric fluorescence," Phys. Rev. A **64,** 023802 (2001).

[17] D. Ljunggren and M. Tengner, "Optimal focusing for maximal collection of entangled narrow-band photon pairs into single-mode fibers," Phys. Rev. A **72,** 062301 (2005).

[18] J. Peatross and M. Ware, *Physics of Light and Optics* (http://optics.byu.edu/, 2006).